



Magnetic ordered mesoporous copper ferrite as a heterogeneous Fenton catalyst for the degradation of imidacloprid

Yanbin Wang^a, Hongying Zhao^b, Mingfang Li^b, Jiaqi Fan^b, Guohua Zhao^{a,b,*}

^a School of Materials Science and Engineering, Tongji University, 4800 Caan Road, Shanghai 201804, PR China

^b Department of Chemistry, Tongji University, 1239 Siping Road, Shanghai 200092, PR China

ARTICLE INFO

Article history:

Received 20 May 2013

Received in revised form 10 August 2013

Accepted 17 September 2013

Available online 25 September 2013

Keywords:

Ordered mesoporous

Copper ferrite

Heterogeneous Fenton catalysis

Imidacloprid

ABSTRACT

Highly ordered mesoporous copper ferrite (meso-CuFe₂O₄) with high surface area and large pore size was successfully fabricated and firstly proposed as a heterogeneous Fenton catalyst. It was synthesized through the nanocasting strategy by using KIT-6 as hard template. The morphology and physicochemical properties of meso-CuFe₂O₄ were characterized by SEM, TEM, XRD, XPS, FT-IR, Raman spectra, etc. The obtained results showed that the surface area and the pore size of meso-CuFe₂O₄ were 122 m² g⁻¹ and 9.2 nm, respectively. The meso-CuFe₂O₄ presented excellent catalytic activity for the degradation of imidacloprid, achieving almost complete removal of 10 mg L⁻¹ imidacloprid after 5 h at the reaction conditions of 0.3 g L⁻¹ catalyst and 40 mM H₂O₂. Kinetic analysis showed that the degradation of imidacloprid follows the pseudo-first order. The apparent rate constant for meso-CuFe₂O₄ was 1.0445 h⁻¹, which was 1.5, 2 and 2.5 times than those of meso-CoFe₂O₄, con-CuFe₂O₄ and nano-Fe₃O₄, respectively. The amount of hydroxyl radical (•OH) generated was directly proportional to the degradation efficiency of imidacloprid, suggesting the involvement of •OH in oxidizing imidacloprid. The obtained results indicated that meso-CuFe₂O₄ presented the highest activity, which was not only due to its ordered mesoporous structure with high surface area and large pore size, but also assigned to the redox recycle of Fe²⁺/Fe³⁺ and Cu⁺/Cu²⁺ in meso-CuFe₂O₄. The special effect of Cu was discussed in terms of the thermodynamically favorable Fe³⁺ reduction by Cu⁺, regenerating the active species Fe²⁺. The meso-CuFe₂O₄ presented very low iron leaching (<1 ppm) even in acidic condition and retained almost its high catalytic activity after 5 consecutive runs. Besides, meso-CuFe₂O₄ possessed medium saturation magnetization, which had provided a potential advantage for the recovery and reuse of catalyst.

© 2013 Elsevier B.V. All rights reserved.

1. Introduction

Fenton technology is one of the powerful and widely used advanced oxidation processes (AOPs) for the treatment of industrial wastewater containing non-biodegradable organic pollutants. However, the classical homogeneous Fenton process has two significant defects: (i) limited by a narrow pH range (pH 2–3); (ii) producing a large iron sludge at the end of process, which increases the cost for the treatment of wastewater. To overcome these drawbacks of homogeneous Fenton, heterogeneous Fenton-like catalysis has been developed [1]. In the past decades, the potential applications of heterogeneous catalysts have been investigated widely. Various kinds of iron oxides and iron hydroxides, such as Fe₃O₄, α-Fe₂O₃ and α-FeOOH have already been used to catalyze the decomposition of organic pollutants. However,

many of them presented weak catalytic activity [2], which limited the practical application of heterogeneous Fenton-like catalysts. Moreover, the leaching of Fe contents from the bulk catalysts to the solution and the difficulty to separate them from the treated water leads to depletion of their catalytic activity in the long term [3]. Therefore, to fabricate a catalyst with higher activity, better stability and reusability is the goal of the scientists who are dedicating to heterogeneous Fenton-like catalysis.

Recently, various strategies have been developed to enhance the activity of heterogeneous Fenton catalyst, e.g. reducing the size of catalyst to nano-scales to increase the surface energy [4], loading the catalysts on carriers with high surface area to improve their dispersion [5], and introducing suitable transition metal (such as Ti, Co, Mn, Cr and V) into the structure of Fe₃O₄ to enhance the catalytic activity [6–13]. Particularly, the last one has been paid more attention due to the fact it could significantly improve the activity of catalysts. For example, Costa et al. [6,7] reported that the isomorphic substitution of Fe²⁺ by Co²⁺ and Mn²⁺ can remarkably increase the activity of Fe₃O₄. In addition, the stability and reusability of catalysts are also important for their practical application in the

* Corresponding author at: Department of Chemistry, Tongji University, 1239 Siping Road, Shanghai 200092, PR China. Tel.: +86 21 65981180; fax: +86 21 65982287.

E-mail address: g.zhao@tongji.edu.cn (G. Zhao).

treatment of waste water. In previous reports, the stability of catalyst could be increased by modifying the surface of catalyst with inorganic or organic substance [14,15]. And the issue that catalysts are difficult to separate from the treated water could be solved by using magnetic materials as heterogeneous catalyst [16,17]. If one material possesses the advantages of high reactivity, good stability and ability to be magnetically separated, it can be applied in a wide range of fields.

Copper ferrite, CuFe_2O_4 , is a magnetic spinel material with cubic structure. Due to its medium saturation magnetization, excellent chemical stability and mechanical strengths, CuFe_2O_4 has already attracted extensive attention in the potential applications such as water gas shift reaction, CO oxidation, decomposition of gaseous pollutants and other reactions [18]. Recently, Zhang and Ding et al. [19,20] reported nanoscaled magnetic CuFe_2O_4 as a heterogeneous catalyst for the catalytic activation of peroxyxonosulfate to generate sulfate radicals. However, the surface area of CuFe_2O_4 MNPs (magnetic nanoparticles) prepared by solid phase synthesis or sol-gel combustion method was very low (usually lower than $10 \text{ m}^2 \text{ g}^{-1}$). Such a low ratio of surface area to mass imposes limits on the resulting material's catalytic activity and applicability. This problem might be solved by fabricating heterogeneous catalyst with porous structure. As we all know, ordered mesoporous materials are ideal candidate as heterogeneous catalyst not only because of their high surface area but also the large pore in their structure network. The mesopore of 2–50 nm is in favor of the adsorption of the macromolecules and can largely reduce the mass transfer resistance [21]. For instance, Su et al. [22] synthesized mesoporous zinc ferrite by a hydrothermal process and used it as photocatalyst toward the degradation of Acid Orange II. Sahoo et al. [23] reported magnetic mesoporous manganese ferrite nanocomposites which were used as a catalyst for the degradation of methyl orange dye.

In this work, highly ordered mesoporous CuFe_2O_4 was synthesized through the nanocasting strategy and used as a powerful candidate of heterogeneous Fenton-like catalyst for the degradation of imidacloprid. Imidacloprid, one of the insecticides most used in agricultural areas, was selected as a model pollutant for evaluating the catalytic activity of spinel catalyst, because it is highly soluble in water (0.58 g L^{-1}) and remains stable in it for more than 30 days [24]. The main purpose of this study is to elucidate the effect of ordered mesoporous structure and the role of copper and iron on the catalytic activity of CuFe_2O_4 in the heterogeneous Fenton reaction. For comparison, ordered mesoporous CoFe_2O_4 synthesized by the same method, conventional CuFe_2O_4 synthesized by solid-phase method and Fe_3O_4 were prepared as reference catalysts. Additionally, the possible mechanism was proposed on the basis of the detected $\cdot\text{OH}$ radical and the surface reaction revealed by comprehensive characterizations. Finally, the stability and reusability of the catalyst was evaluated.

2. Experimental

2.1. Reagents

Tetraethylorthosilicate (TEOS), ferric nitrate ($\text{Fe}(\text{NO}_3)_3 \cdot 9\text{H}_2\text{O}$), copper nitrate ($\text{Cu}(\text{NO}_3)_2 \cdot 3\text{H}_2\text{O}$), cobalt nitrate ($\text{Co}(\text{NO}_3)_2 \cdot 6\text{H}_2\text{O}$), butyl alcohol, hydrochloric acid (HCl), sodium hydroxide (NaOH), *n*-hexane for preparation of ordered mesoporous CuFe_2O_4 and CoFe_2O_4 were obtained from Sinopharm Chemical Reagent Co., Ltd., SCRC, China. H_2O_2 (30%, v/v), ethanol, isopropanol and imidacloprid (IMI) were supplied by Aladdin Co., China. Triblock copolymer Pluronic P123 ($M_w = 5800$, EO₂₀PO₇₀EO₂₀) was purchased from Sigma–Aldrich. All of the chemicals were reagent grade and used as received without further purification. Deionized water was used in all the experiments.

2.2. Preparation of samples

KIT-6 was synthesized according to the previous literature [25]. Highly ordered mesoporous CuFe_2O_4 and CoFe_2O_4 (denoted as meso- CuFe_2O_4 and meso- CoFe_2O_4 , respectively) were prepared through the nanocasting strategy [26], using the as-prepared KIT-6 as hard templates. The classical procedure for preparing meso- CuFe_2O_4 was carried out as follows: firstly, 0.288 g $\text{Cu}(\text{NO}_3)_2 \cdot 6\text{H}_2\text{O}$ and 0.962 g $\text{Fe}(\text{NO}_3)_3 \cdot 9\text{H}_2\text{O}$ were per-mixed together with 0.5 g as-prepared KIT-6 powder and ground in an agate mortar in the presence of 10 mL of *n*-hexane to yield a homogeneous mixture. Afterwards, the resulting mixture was subsequently dispersed in 30 mL *n*-hexane and stirred overnight under reflux at 70 °C. After cooling down, the solid products were recovered by filtration, dried in an oven at 70 °C and calcined in a tubular furnace under air atmosphere with the heating rate of 1 °C min⁻¹, then keeping the temperature at 600 °C for 5 h. Finally, the silica template was selectively dissolved by 2 M NaOH solution in 60 °C water bath under continuously vigorous stirring for 24 h, and the brown product was obtained by washing with distilled water and ethanol for three times and drying at vacuum oven. The meso- CoFe_2O_4 was fabricated in the same way. And the conventional CuFe_2O_4 and CoFe_2O_4 without mesoporous structure (denoted as con- CuFe_2O_4 and con- CoFe_2O_4) were prepared by using the traditional solid-phase method, the specific steps are as follows: the corresponding mixture in stoichiometric proportion of the $\text{Cu}(\text{NO}_3)_2 \cdot 6\text{H}_2\text{O}$, $\text{Fe}(\text{NO}_3)_3 \cdot 9\text{H}_2\text{O}$ and $\text{Co}(\text{NO}_3)_2 \cdot 6\text{H}_2\text{O}$ were calcined at 600 °C for 5 h with a heating rate of 1 °C min⁻¹ in air atmosphere. The Fe_3O_4 magnetic nanoparticles were synthesized by the chemical coprecipitation method [27] as previously reported in the literature, and the product was denoted as nano- Fe_3O_4 .

2.3. Characterization methods

Power X-ray diffraction (XRD) patterns were measured on a Bruker D8 Advance X-ray diffractometer using Cu K α ($\lambda = 1.540562 \text{ \AA}$, 40 kV, 40 mA) as the X-ray source. The high-resolution transmission electron microscopy (HR-TEM) images were obtained on a JEOL JEM-2100 transmission electron microscope. The scanning electron microscopy (SEM) images were obtained on a Hitachi S-4800 scanning electron microscope. N_2 adsorption–desorption analysis was measured on a Micromeritics TriStar 3000 instrument, Brunauer–Emmet–Teller (BET) specific surface area was estimated from the relative pressure range from 0.05 to 0.20, pore volumes were determined using the adsorbed volume at a relative pressure of 0.99033, and the pore size distributions of the as-prepared samples were analyzed using the Barrett–Joyner–Halenda (BJH) method from the desorption branch of the N_2 adsorption–desorption isotherm. Fourier transform infrared spectra (FT-IR) were collected in the region from 400 to 4000 cm^{-1} at room temperature using a Nicolet 6700 spectroscopy on KBr pellets. Raman spectroscopy was performed by a Renishaw Raman microspectrometer using an Ar⁺ ion laser (514.5 nm line) as the excitation source. X-ray photoelectron spectroscopy was recorded on a Kratos ASIS-HS X-ray photoelectron microscope equipped with a standard and monochromatic source (Al K α) operated at 150 W (15 kV, 10 mA). H₂-TPR measurements were performed using AutoChem II 2920 instrument (Micromeritics). Prior to the TPR run, the fresh sample was pretreated in situ for 1 h at 200 °C in air flow. After cooling and a step of purge of the lines in Ar flow, an H₂:Ar mixture (H₂:Ar volume ratio of 10% and total flow of 50 mL min⁻¹) was sent through the sample while increasing the temperature up to 800 °C with a rate of 10 °C min⁻¹. Finally, the magnetic properties were measured by a Lakeshore 735 vibrating sample magnetometer (VSM) at room temperature.

2.4. Experimental procedure

Batch degradation experiments of imidacloprid were carried out in a beaker (100 mL) at 30 °C. The initial concentration of target substance was 10 mg L⁻¹, and the total volume of reaction solution was 50 mL. The reaction suspension was prepared by adding the required amount of catalyst into 50 mL of a 10 mg L⁻¹ imidacloprid solution that had been adjusted to the desired pH value by 0.1 M H₂SO₄. A known concentration of H₂O₂ was added to the solution to initiate the reaction. Samples were taken at set intervals using a 5 mL syringe, filtered immediately through a 0.22 µm filter film, and quenched with excess isopropanol. To evaluate the contribution of homogeneous Fenton catalyzed by the leaching Fe and Cu ions on the imidacloprid degradation, experiment was carried out as follows: after mixing meso-CuFe₂O₄ with imidacloprid solution (pH 3.0) for 5 h and removing the catalyst by filtering, 204 µL H₂O₂ (30 wt%) was added into the filtrate. The reusability of the catalyst was evaluated by collecting the catalyst with a magnet, washing with deionized water, drying the used catalyst under vacuum, and using it for the next reaction under similar experimental conditions.

2.5. Sample analysis

Quantitative analysis of imidacloprid during the reaction was carried out by high performance liquid chromatography (HPLC), a Varian Prostar 310 system equipped with Varian AQ-C18 column (4.6 mm × 150 mm × 5 µm) and a diode array UV-vis detector (DAD). The mobile phase was a mixture of methanol and water (30:70, v/v) with a flow rate of 1.0 mL min⁻¹, the injection volume was 20 µL, and the UV detector was operated at 270 nm.

The quantitation of hydroxyl radicals were determined with the method which was reported in the previous literatures [28]. The concentration of ferrous ion leaching and total iron leaching were measured according to the 1,10-phenanthroline method [29], and the absorbance was measured at 510 nm using a UV-vis spectrophotometer (Agilent, 8453) with a 1 cm path length spectrometric quartz cell. Total organic carbon values were determined by

a Multi 3100 TOC/TN analyzer (Analytik Jena AG Corporation). For TOC analysis, all the samples were immediately treated with scavenging reagent (0.1 M Na₂SO₃, 0.1 M KH₂PO₄, 0.1 M KI and 0.05 M NaOH) to obtain accurate TOC values [30,31].

GC/MS analysis was employed to identify by-products formed during the imidacloprid degradation process. Prior to GC/MS analysis, the samples were pretreated by liquid–liquid extraction with CHCl₃ solvent to extract and concentrate by-products. Then, the extracts were dried with anhydrous sodium sulfate overnight. Finally, the extracts were concentrated using rotary evaporator at 40 °C down to 1 mL for analyzing. Spectra were obtained with a gas chromatograph (Agilent 7890A), equipped with DB-5 MS capillary column (30 mm × 320 µm, 0.5 µm film thickness), interfaced directly to the mass spectrometer (5975A inert XL MSD with Triple-Axis Detector) used as a detector. GC/MS analysis was performed according to the following conditions: the column oven was initially set at 60 °C for 2 min, subsequently ramped to 100 °C with 6 °C min⁻¹ rate, then to 200 °C with 10 °C min⁻¹ rate and finally to 285 °C with 20 °C min⁻¹ rate, where it was held for 5 min. Injector temperature was 250 °C with helium served as the carrier gas at the flow rate of 1 mL min⁻¹. Electron impact (EI) mode at 70 eV was used and the mass range scanned was 10–400 m/z.

3. Results and discussion

3.1. The fabrication, morphology and physicochemical properties of catalysts

Fig. 1 illustrates the fabrication process of ordered mesoporous copper ferrite using the hard template method. The process including three main steps: firstly, the KIT-6 template was infiltrated with the precursor of ferric nitrate and copper nitrate by grounding and refluxing the mixture in the presence of n-hexane; subsequently, the mixture was calcined at the desired temperature under air atmosphere, therefore, the precursor inside the pores of KIT-6 was converted to copper ferrite by decomposition inside the pores of KIT-6; finally, the mesoporous silica template was selectively

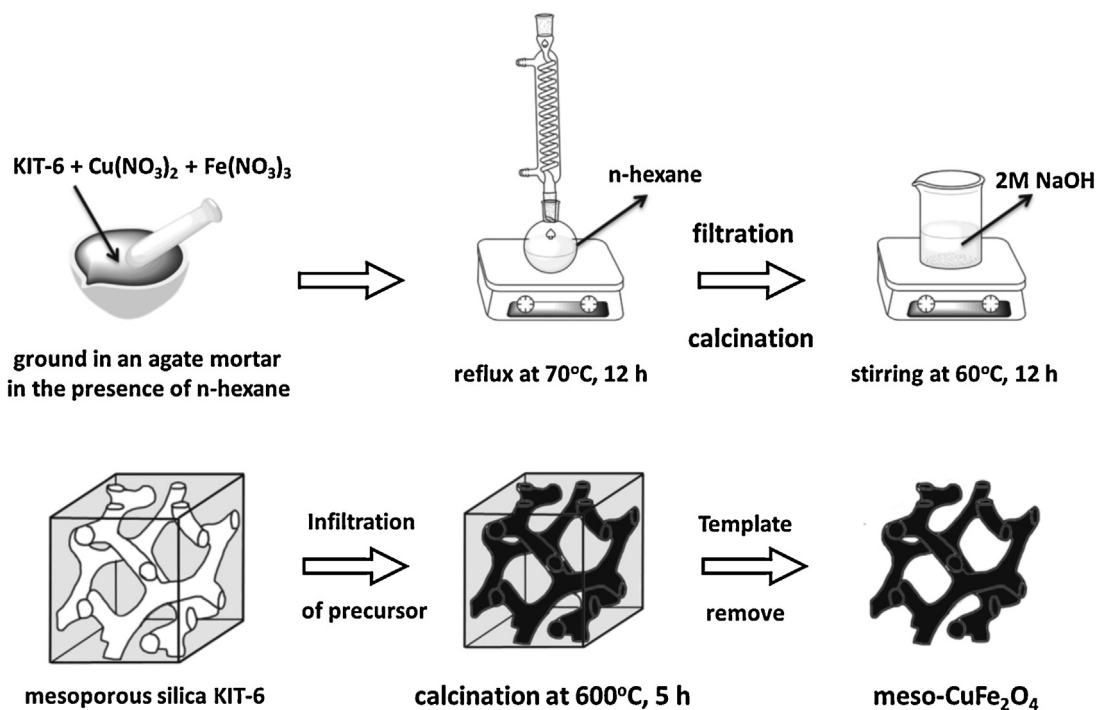


Fig. 1. Schematic illustration of the fabrication of magnetic meso-CuFe₂O₄.

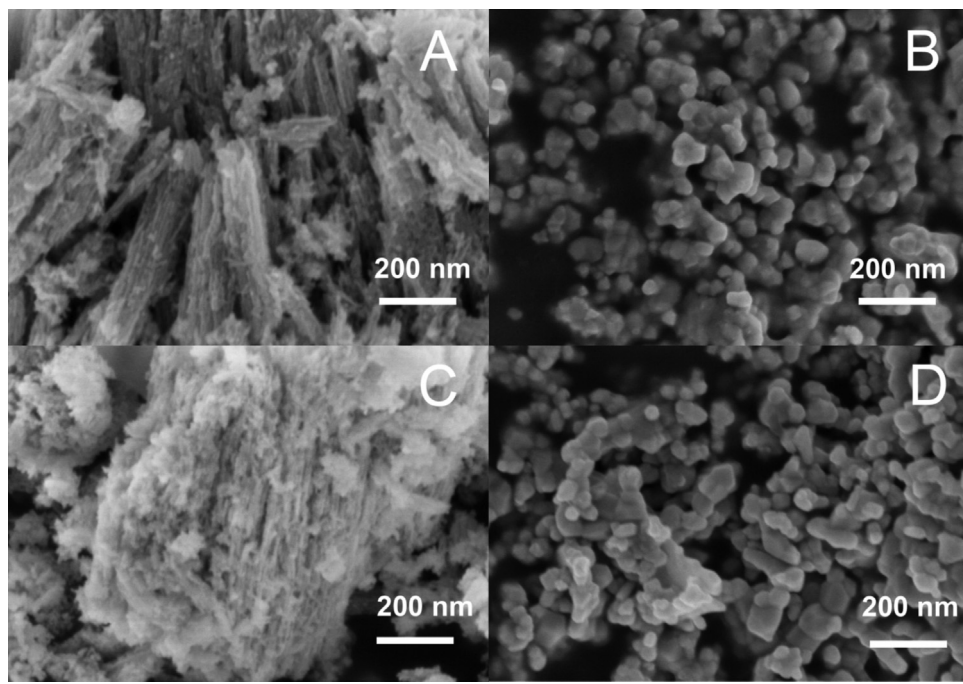


Fig. 2. SEM images of meso-CuFe₂O₄ (A), con-CuFe₂O₄ (B) meso-CoFe₂O₄ (C) and con-CoFe₂O₄ (D).

removed using aqueous NaOH solution, and after washing, the material replicating the mesostructure of KIT-6 was obtained.

In order to understand the structure–performance relationship, the morphology of as-prepared catalysts was characterized by SEM. Fig. 2 presents SEM images illustrating the morphology of as-prepared catalysts. It can be seen that the morphology of these synthesized meso-CuFe₂O₄ and meso-CoFe₂O₄ (Fig. 2A and C) are very different from con-CuFe₂O₄ and con-CoFe₂O₄ (Fig. 2B and D), the former have an obvious porous structure while the latter were composed of particles with diameter of 50–150 nm. The porous structure of the as-prepared meso-CuFe₂O₄ and meso-CoFe₂O₄ originates from the structure of KIT-6 template. To further investigate the mesostructure of meso-CuFe₂O₄ and meso-CoFe₂O₄, the samples were characterized by TEM. The TEM images of KIT-6 are depicted in Fig. 3A and B. It can be estimated from Fig. 3B that the pore size of KIT-6 template is about 6.8 nm, which is consistent with the previous reported value [25]. The well-ordered mesoporous structure of meso-CuFe₂O₄ and meso-CoFe₂O₄ are clearly visible in Fig. 3C and E, which demonstrates the catalysts are successfully replicated from the KIT-6 silica template. The pore size of meso-CuFe₂O₄ and meso-CoFe₂O₄ are 2.3 and 3.4 nm, respectively. The high-resolution transmission electron microscopy of meso-CuFe₂O₄ and meso-CoFe₂O₄ are shown in Fig. 3D and F. The observed lattice fringes indicated that the meso-CuFe₂O₄ and meso-CoFe₂O₄ produced by the confinement effect within mesoporous silica are nano-crystalline. In the case of meso-CuFe₂O₄ and meso-CoFe₂O₄ with crystalline walls, the lattice repeat, a_0 , is 0.242 and 0.289 nm, corresponding to the (202) and (220) crystal face of CuFe₂O₄ and CoFe₂O₄.

Wide-angle XRD is used to identify the crystalline phase of the samples and the results are shown in Fig. 4. Fig. 4A and B shows the XRD patterns of meso-CuFe₂O₄ and con-CuFe₂O₄. The 2 θ values at 18.36°, 29.98°, 34.69°, 35.66°, 37.21°, 43.84°, 58.14° and 62.33°, could be indexed to the (101), (112), (103), (211), (202), (220), (321) and (224) planes of a face-centered cubic CuFe₂O₄ (JCPDS No.34-0425). It is clear to see that the peaks of meso-CuFe₂O₄ is relatively broader than the peaks of con-CuFe₂O₄, possibly due to the pore walls were composed of small particles. Fig. 4C and D displays the XRD patterns of meso-CoFe₂O₄ and con-CoFe₂O₄. The 2 θ

values at 18.38°, 30.16°, 35.54°, 37.18°, 43.19°, 53.59°, 57.10° and 62.66°, could be indexed to the (111), (220), (311), (222), (400), (422), (511) and (440) planes of a face-centered cubic CoFe₂O₄ (JCPDS No. 22-1086). No impurity peaks are observed, indicating that the samples obtained via nanocasting method consist of single phases. According to the full width at the half-maximum of the diffraction peak, the average crystallite size of meso-CuFe₂O₄ and meso-CoFe₂O₄ can be calculated to be 5.3 and 7.8 nm, respectively, using the Scherrer equation:

$$D_{hkl} = \frac{K\lambda}{\beta_{hkl} \cos \theta_{hkl}}$$

where D_{hkl} is the crystallite size perpendicular to the normal line of the (hkl) plane, K a constant (0.89), β_{hkl} the full width at half-maximum (fwhm) of the (hkl) diffraction peak, θ_{hkl} the Bragg angle of the (hkl) peak, and λ the X-ray wavelength.

Textural properties of ordered mesoporous catalysts were investigated by nitrogen sorption analysis. The nitrogen adsorption–desorption isotherms and the pore size distribution of meso-CuFe₂O₄ and meso-CoFe₂O₄ are exhibited in Fig. 5. The corresponding parameters including BET surface area, pore volume and average pore size are listed in Table 1. The isotherms show that both meso-CuFe₂O₄ and meso-CoFe₂O₄ give type IV isotherms and type H3 hysteresis loop, with the hysteresis shaping more like that for the slit pores and covering a broad relative pressure range, starting from about 0.6 and extending almost to 0.95, indicating their large porosity [32]. The BET surface area of the meso-CuFe₂O₄ and meso-CoFe₂O₄ are 122 m² g⁻¹ and 101 m² g⁻¹, 30 and 9 times than those of con-CuFe₂O₄ and con-CoFe₂O₄ ($S_{\text{con-CuFe}_2\text{O}_4} = 4 \text{ m}^2 \text{ g}^{-1}$, and $S_{\text{con-CoFe}_2\text{O}_4} = 11 \text{ m}^2 \text{ g}^{-1}$), respectively. This observation suggests that the BET surface areas are significantly improved by fabricating mesoporous structure through the nanocasting strategy. Moreover, the average pore sizes of meso-CuFe₂O₄ and meso-CoFe₂O₄ are 9.2 and 9.5 nm, and the large pore size is benefit to the adsorption and mass transfer of large molecules.

In order to get a further understanding about the physico-chemical characteristics of as-prepared catalysts, FT-IR and Raman spectra were used to examine the surface properties of samples.

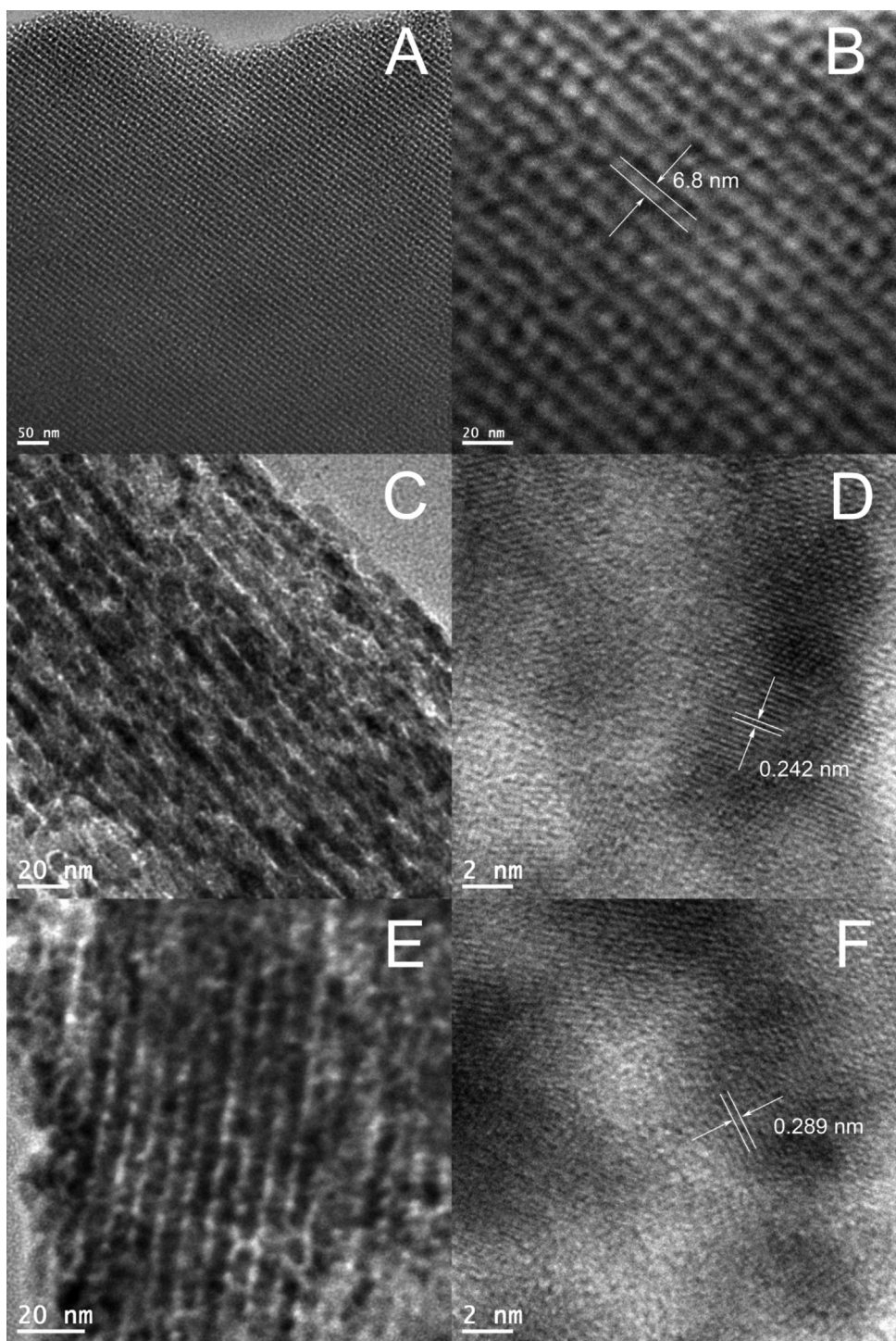


Fig. 3. TEM images of KIT-6 (A and B), meso-CuFe₂O₄ (C and D) and meso-CoFe₂O₄ (E and F) with crystalline walls.

Table 1

BET surface area, pore volume, pore size and magnetic properties of different samples.^a

Samples	BET surface area (m ² g ⁻¹)	Pore volume (cm ³ g ⁻¹)	Pore size (nm)	<i>H</i> _c (Oe)	<i>M</i> _s (emu g ⁻¹)	<i>M</i> _r (emu g ⁻¹)
KIT-6	565	1.16	6.8	–	–	–
Meso-CoFe ₂ O ₄	101	0.37	9.5	288.45	27.586	4.4045
Meso-CuFe ₂ O ₄	122	0.37	9.2	19.179	15.448	0.21461
Con-CoFe ₂ O ₄	11	0.04	–	1336.8	52.93	22.050
Con-CuFe ₂ O ₄	4	0.04	–	973.39	13.352	5.7916
Nano-Fe ₃ O ₄	135	0.18	3.9	3.7096	28.159	0.10095

^a Pore volume was measured at the relative pressure of 0.99, average pore diameter was calculated from the adsorption branch by BJH method; saturation magnetization (*M*_s), remanent magnetization (*M*_r), and coercivity (*H*_c) were measured at room temperature.

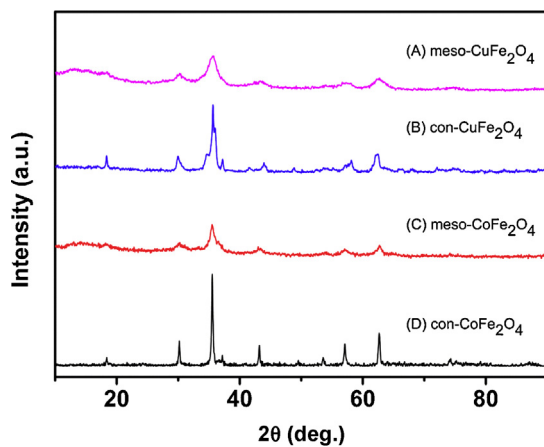


Fig. 4. Wide-angle XRD patterns of meso-CuFe₂O₄ (A), con-CuFe₂O₄ (B), meso-CoFe₂O₄ (C) and con-CoFe₂O₄ (D).

It can be seen in Fig. 6 that meso-CuFe₂O₄ and con-CuFe₂O₄ had two absorption peaks at $\sim 585\text{ cm}^{-1}$ and $\sim 420\text{ cm}^{-1}$. According to the geometrical configuration of the oxygen nearest neighbor, the metal ions in ferrite can be situated in two different sublattices, namely tetrahedral (A-sites) and octahedral (B-sites) [31]. In inverse copper ferrite, the peak at $\sim 585\text{ cm}^{-1}$ is due to the vibrations of Fe³⁺-O²⁻ complexes situated at A-sites and $\sim 420\text{ cm}^{-1}$ is due to Cu²⁺-O²⁻ complexes at B-sites [33]. While for meso-CoFe₂O₄ and con-CoFe₂O₄, both of them had a broad adsorption at around 590 cm^{-1} , which was the stretching of Co-O in tetrahedral sites and was typical for CoFe₂O₄ molecules [32,34]. And the typical adsorptions peaks of Fe₂O₃ (about 540 and 470 cm^{-1}) [35] and CuO (around 405 , 433 , 497 , 529 , and 603 cm^{-1}) [36] are not observed. These results confirm that the synthesized products are single phase CuFe₂O₄ and CoFe₂O₄, which is in agreement with the XRD results.

The Raman spectra of the synthesized materials are shown in Fig. 6. The peaks of con-CuFe₂O₄ are located at 156 , 275 , 465 and 677 cm^{-1} , which is consistent with the previous report [37]. However, it can be clearly seen that the peaks of meso-CuFe₂O₄ shift to lower frequencies situated at 145 , 273 , 459 and 667 cm^{-1} , respectively. This phenomenon is also been observed for CoFe₂O₄ system. For con-CoFe₂O₄, it presents three strong peaks located at 686 , 462 and 301 cm^{-1} , and two weak peaks at $\sim 615\text{ cm}^{-1}$ and 198 cm^{-1} [37], and the corresponding peaks of meso-CoFe₂O₄ were shifted

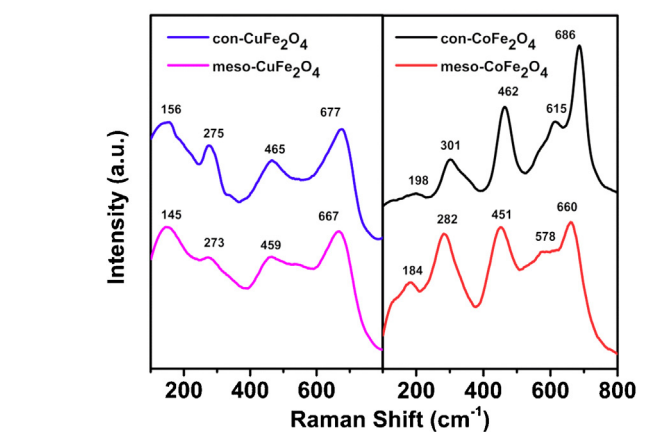
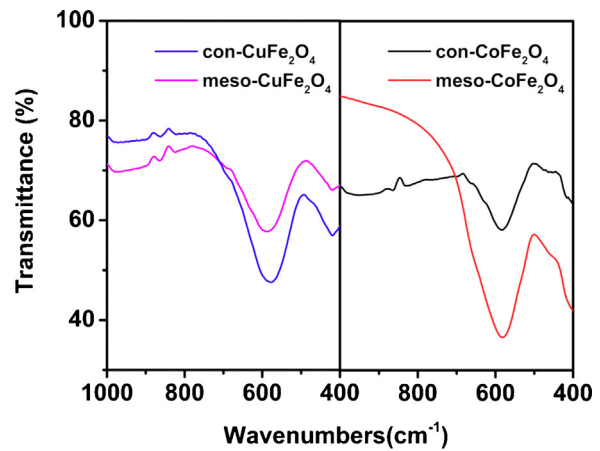


Fig. 6. FT-IR and Raman spectra of different catalysts. (For interpretation of the references to color in this figure legend, the reader is referred to the web version of this article.)

to 660 , 451 , 282 , 578 and 184 cm^{-1} , respectively. The difference between the spectra is attributed to the smaller size and particular mesoporous wall of meso-CuFe₂O₄ and meso-CoFe₂O₄ [38,39], and the result is consistent with XRD and TEM.

3.2. Efficient catalytic degradation performance on imidacloprid and plausible mechanism

The catalytic activity of as-prepared catalysts was investigated by performing experiments on the degradation of 10 mg L^{-1} imidacloprid at the conditions of H_2O_2 40 mM , catalyst dosage 0.3 g L^{-1} , pH at 3.00 and T at 30°C . The degradation results were shown in Fig. 7. As can be seen from Fig. 7, three conclusions could be summarized. Firstly, the catalytic activity of catalysts with ordered mesoporous structure is superior to non-mesoporous structure (e.g. meso-CuFe₂O₄ > con-CuFe₂O₄, meso-CoFe₂O₄ > con-CoFe₂O₄). The excellent catalytic activity of catalysts with ordered mesoporous structure is assigned to the mesoporous network structure and large pore size. That is to say, for mesoporous catalysts, not only the higher surface area is beneficial to raise the number of active sites of catalysts, but also the larger pore size contribute to reduce the mass transfer resistance and promote the heterogeneous Fenton reaction. Secondly, the catalytic activity of CuFe₂O₄ is superior to CoFe₂O₄ (e.g. meso-CuFe₂O₄ > meso-CoFe₂O₄, con-CuFe₂O₄ > con-CoFe₂O₄). Thirdly, the catalytic activity of catalysts with ordered mesoporous structure is superior to conventional catalyst such as Fe₃O₄ (meso-CuFe₂O₄ > meso-CoFe₂O₄ > Fe₃O₄). Specially,

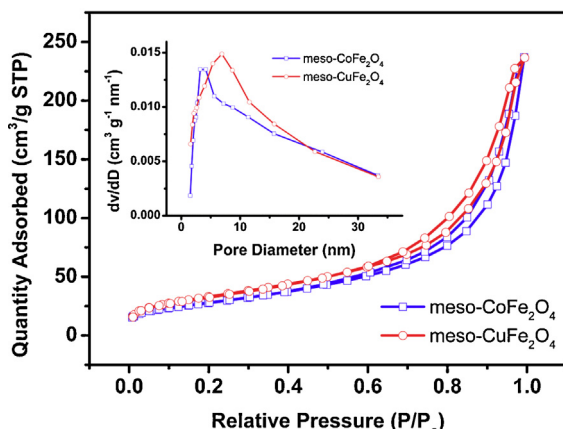


Fig. 5. N₂ adsorption-desorption isotherms measured at 77 K and pore size distributions from the desorption branches through the BJH method (inset) of meso-CuFe₂O₄ (red line) and meso-CoFe₂O₄ (blue line). (For interpretation of the references to color in this figure legend, the reader is referred to the web version of this article.)

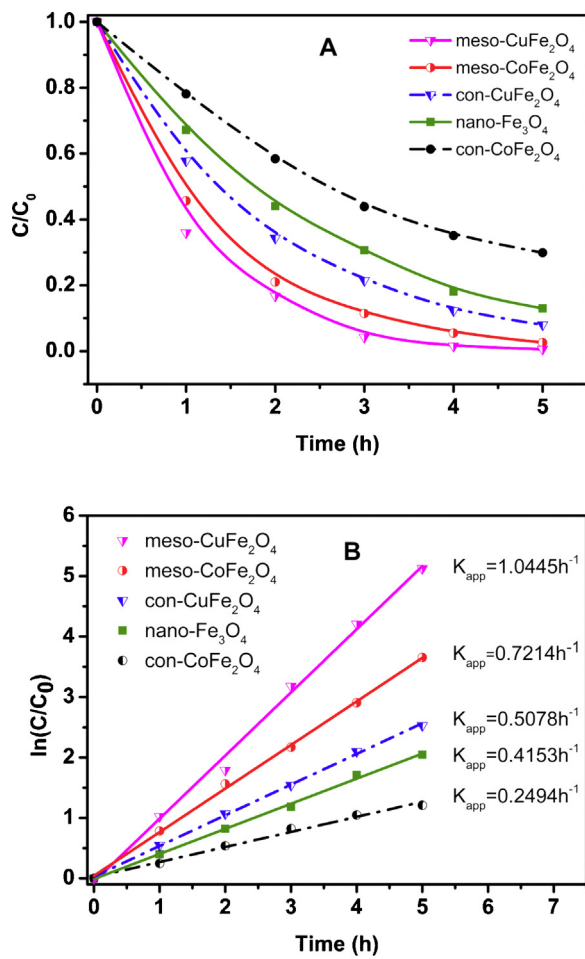


Fig. 7. The removal efficiency of imidacloprid with different catalysts during the reaction in 5 h, at pH 3.00 with 40 mM H₂O₂, 0.3 g L⁻¹ catalyst dosage, and 10 mg L⁻¹ imidacloprid (A); the kinetic analysis of imidacloprid degradation, that is the dependence of ln(C₀/C) versus time (B).

meso-CuFe₂O₄ presents the best catalytic activity and the removal efficiency of imidacloprid is nearly 100% after 5 h.

Moreover, the data for imidacloprid concentration decay were further analyzed by kinetic equation. The kinetics equation may be expressed as

$$\ln \left(\frac{C_0}{C} \right) = k't$$

where k' is the apparent reaction constant and C_0 and C are the initial concentration and the concentration at time t , of imidacloprid, respectively. The pseudo-first order reaction kinetics was obviously observed and applied well to all experiments (see Fig. 7B). The apparent rate constant of meso-CuFe₂O₄ is 1.0445 h⁻¹, which is 1.45, 2 and 4 times than meso-CoFe₂O₄, con-CuFe₂O₄ and nano-Fe₃O₄, respectively.

It is well known that traditional homogeneous Fenton is a powerful and widely studied method for treating organic pollutants. To accurately estimate the catalytic activity of meso-CuFe₂O₄, comparable amounts of FeSO₄ was used to catalyze the degradation of imidacloprid. The results show that 10 mg L⁻¹ imidacloprid could be completely removed in 1 h (the data not shown). Although traditional Fenton represents highly removal efficiency for imidacloprid and the reagent of FeSO₄ is cheap, a lot of yellow precipitates formed at the end of process. Therefore, the precipitates must be separated and the catalyst could not be recycled, which indisputably increase the cost for the treatment of iron sludge and

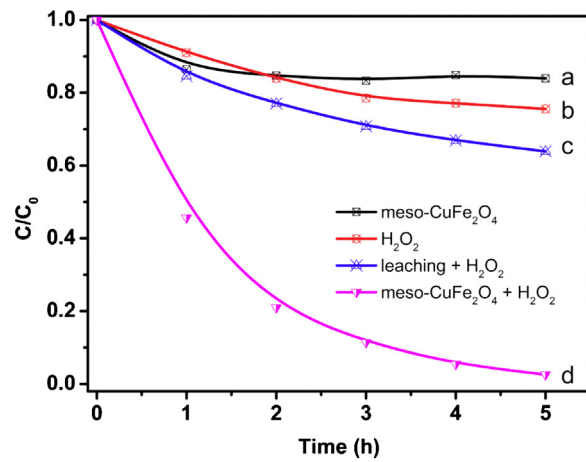


Fig. 8. The removal efficiency of imidacloprid in the presence of (a) meso-CuFe₂O₄, (b) H₂O₂, (c) leaching Fe and Cu ions + H₂O₂ and (d) meso-CuFe₂O₄ + H₂O₂.

strongly limit the application of traditional Fenton. In comparison, the materials used to synthesized meso-CuFe₂O₄ are not expensive. Moreover, meso-CuFe₂O₄ could be recycled and remains high catalytic activity even after several runs. In this respect, using meso-CuFe₂O₄ as catalyst is relatively 'cheap'.

To evaluate the adsorption effect of imidacloprid by meso-CuFe₂O₄, adsorption experiments were conducted under the same experimental conditions that those employed for catalytic runs with heterogeneous Fenton catalysts. As shown in Fig. 8, the adsorption of imidacloprid by meso-CuFe₂O₄ up to 9%, which is due to meso-CuFe₂O₄ possesses high specific surface area (122 m² g⁻¹). The meso-CuFe₂O₄ shows good capacity of adsorption for imidacloprid, which is benefit of the reaction between imidacloprid and hydroxyl radical generated on the surface of heterogeneous Fenton catalyst. Thus, meso-CuFe₂O₄ represents the better catalytic activity for the degradation of imidacloprid than con-CuFe₂O₄.

To investigate the contribution of homogeneous Fenton reaction catalyzed by the leaching Fe and Cu ions on the imidacloprid degradation, experiment in homogeneous systems was carried out by removing meso-CuFe₂O₄ catalyst after vigorous agitation for 5 h and then adding 204 μ L H₂O₂ (30 wt.%) into the filtrate. As shown in Fig. 8, the removal of imidacloprid by adsorption was 9%, the removal of imidacloprid by H₂O₂ oxidation (without catalyst added) at 5 h was 24%, while the removal of imidacloprid at 5 h was 36% by homogeneous Fenton-like reaction (catalyzed by the leaching Fe and Cu ions). Therefore, the contribution of homogeneous Fenton-like was about 3%. Nevertheless, the removal of imidacloprid catalyzed by meso-CuFe₂O₄ at 5 h was almost 100%. These results indicated that the contribution of homogeneous Fenton-like reaction was a little, which confirmed the degradation of imidacloprid was mainly dominated by the heterogeneous reaction catalyzed by meso-CuFe₂O₄.

In addition to increasing catalytic activity, another motive to develop new heterogeneous Fenton-like catalyst is to extend the pH range application [40–42]. As shown in Table 2, the catalytic activity

Table 2

Effect of pH values on the imidacloprid removal efficiency (%).^a

Catalyst	pH values			
	3.0	5.0	7.0	9.0
Meso-CuFe ₂ O ₄	98	77	62	54
FeSO ₄	100	22	13	7

^a Reaction conditions: catalyst dosage 0.3 g L⁻¹, initial imidacloprid concentration 10 mg L⁻¹, and initial H₂O₂ concentration 40 mM, reaction for 5 h.

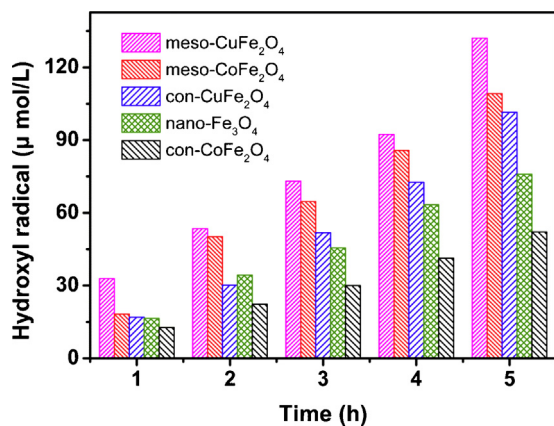


Fig. 9. Total concentrations of $\cdot\text{OH}$ formed as a function of time for 0.3 g L^{-1} catalyst dosage, $40 \text{ mM H}_2\text{O}_2$, and pH 3.00. Benzoic acid used as a probe at 10 mM (meso- CuFe_2O_4 : magenta; con- CuFe_2O_4 : blue; meso- CoFe_2O_4 : red; con- CoFe_2O_4 : black; nano- Fe_3O_4 : olive). (For interpretation of the references to color in this figure legend, the reader is referred to the web version of this article.)

of meso- CuFe_2O_4 was affected by the pH values. With the increase of solution pH from 3.0 to 9.0, the removal efficiency of imidacloprid decrease from 98% to 54%, respectively. However, traditional homogeneous Fenton strongly affected by the system pH values, when the solution pH was over 5, the catalytic activity was apparently decreased. Torres et al. reported that using traditional Fenton to oxidize bisphenol A, when the initial pH was 7.6, there were no significant effect for the removal efficiency of bisphenol A [43]. The reason is that it is easy to form Fe(OH)_3 precipitate ($\text{p}K_{\text{sp}} = 37.4$) at neutral pH, preventing the catalysis reaction proceeding. Thus, compared with traditional Fenton reaction, meso- CuFe_2O_4 could be used over the wider pH range.

It is known that the mineralization rate is much slower than the degradation rate and the mineralization degree represents the realistic potential of the catalyst. Therefore, the investigation of mineralization degree for imidacloprid was additionally performed with TOC measurements. The TOC removal of imidacloprid catalyzed by meso- CuFe_2O_4 after 5 h is 33%, indicating that the intermediates formed during the degradation of imidacloprid are stability and could not be entirely mineralized in 5 h. These results were similar with previous reported results, such as the TOC removal of imidacloprid by photocatalysis after 2 h is only 19% [44], the DOC (dissolved organic carbon) removal of imidacloprid by photo-Fenton using Fe-ZSM5 as catalyst after 800 min is just 43% [45].

As is known to all, $\cdot\text{OH}$ radical is a nonspecific oxidant, which can react with most organic contaminants at near diffusion-limited rates [46]. Thus, the amount of generated $\cdot\text{OH}$ radicals is a crucial parameter for understanding the degradation of imidacloprid in H_2O_2 assisted spinel heterogeneous Fenton-like reaction. In order to deeply understand the mechanism of degradation of imidacloprid, the cumulative amount of $\cdot\text{OH}$ radicals was measured. During the analysis, benzoic acid was chosen as a probe to determine the concentration of $\cdot\text{OH}$. The reaction rate constant of benzoic acid reacting with $\cdot\text{OH}$ in aqueous media is $4.2 \times 10^9 \text{ M}^{-1} \text{ s}^{-1}$ [28]. It was reported that per mole p-HBA was produced quantitatively by 5.87 ± 0.18 moles $\cdot\text{OH}$ [47]. The obtained results were presented in Fig. 9, which shows the amount of $\cdot\text{OH}$ generated by catalysts gradually increase with the reaction time. For instance, the amount of $\cdot\text{OH}$ generated by meso- CuFe_2O_4 is up to the highest value about $130 \mu\text{mol L}^{-1}$ after 5 h. The capacity of different catalysts to generate $\cdot\text{OH}$ is consistent with the removing efficiency tendency of imidacloprid, so the involvement of $\cdot\text{OH}$ in oxidizing imidacloprid is affirmed.

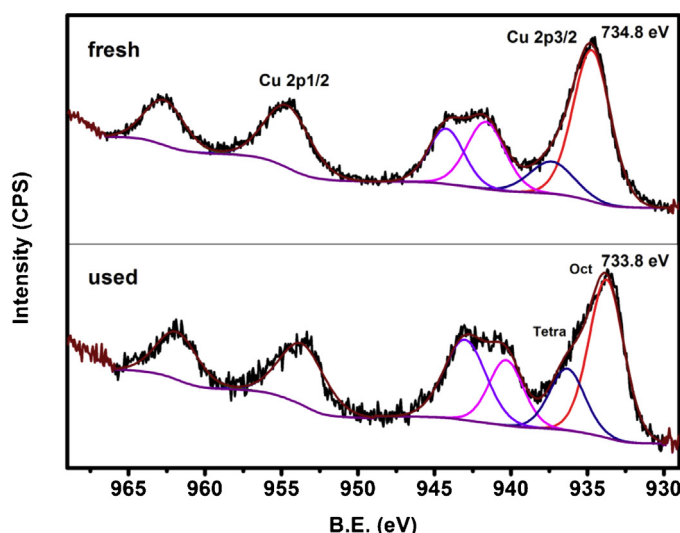
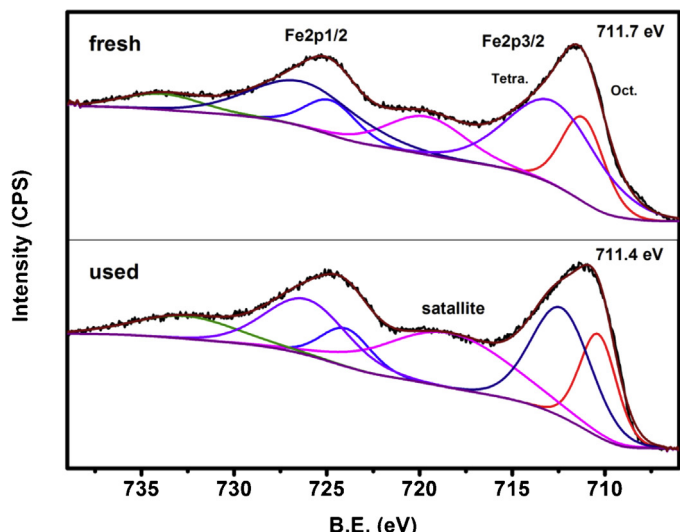


Fig. 10. XPS spectra for Fe 2p regions (top) and Cu 2p regions (bottom) of fresh and used meso- CuFe_2O_4 . (For interpretation of the references to color in this figure legend, the reader is referred to the web version of this article.)

To better understand the roles of copper and iron in Fenton-like catalytic oxidation, XPS spectra of meso- CuFe_2O_4 and meso- CoFe_2O_4 were recorded before and after the degradation experiment of imidacloprid. Fig. 10 shows XPS spectra of Cu 2p and Fe 2p core level regions. As we know, tetragonal CuFe_2O_4 are known to have a spinel structure with virtually complete inversion. In this structure, Cu^{2+} mainly occupy the B-sites, while Fe^{3+} evenly locate both on the A-sites and B-sites [48]. The XPS of Fe 2p regions can be fitted into six contributions (Fig. 10, top). All the Fe 2p spectra display a main peak at around $711.7 \pm 0.5 \text{ eV}$ and a shakeup satellite at around $720.0 \pm 0.5 \text{ eV}$, suggesting the presence of Fe^{3+} cations [13,49]. The presence of the peak around 713.4 and 711.4 eV (for fresh meso- CuFe_2O_4) suggests that Fe^{3+} exist in two coordination environments where A-sites at higher binding energy and B-sites at lower binding energy, respectively [49]. For the XPS of Cu 2p regions, they can be fitted into six contributions. The main peaks at binding energies of $934.76 \pm 0.5 \text{ eV}$ for the $\text{Cu} 2\text{p}_{3/2}$ lines, is assigned to Cu^{2+} on octahedral sites, while the minor ones at $937.36 \pm 0.5 \text{ eV}$ can be assigned to Cu^{2+} on tetrahedral sites [48]. Compared with that for the fresh one, the peaks of $\text{Cu} 2\text{p}_{3/2}$ (934.8 eV) and $\text{Fe} 2\text{p}_{3/2}$ (711.7 eV) for meso- CuFe_2O_4 used in the

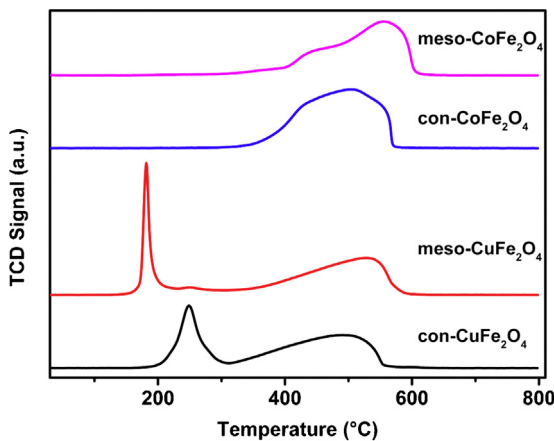


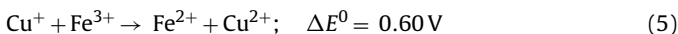
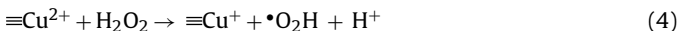
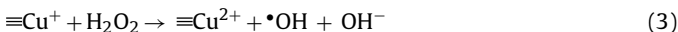
Fig. 11. H_2 -TPR profiles of the different catalysts (TPR conditions: 10% H_2 /Ar with heating rate $10^\circ\text{C min}^{-1}$).

catalytic degradation of imidacloprid, slightly shifted to lower binding energy values of 933.8 eV for Cu $2p_{3/2}$ and 711.4 eV for Fe $2p_{3/2}$, indicating the obvious transformation of Cu(II) to Cu(I) and Fe(III) to Fe(II) after heterogeneous Fenton reaction [40,50].

The mechanism of Fenton-like catalytic oxidation reaction is still far from fully understood. Nevertheless, the most popular candidates that decomposing H_2O_2 to generate $\cdot\text{OH}$ radical can be described in the following reactions [51]:



Similar with Fe^{2+} , Cu^+ also could catalyze H_2O_2 decomposition to generate $\cdot\text{OH}$ radicals and Cu^{2+} may react with H_2O_2 to produce $\cdot\text{HO}_2$ and Cu^+ , the equations are presented as follows [41]:



As described above, the produced $\cdot\text{OH}$ radicals by meso- CuFe_2O_4 was up to $130 \mu\text{mol L}^{-1}$ in 5 h, and the oxidation states of copper and iron on the surface of meso- CuFe_2O_4 partially change from Cu(II) to Cu(I) and Fe(III) to Fe(II) after the reaction. On the basis of the experimental results of the XPS and the measured amount of $\cdot\text{OH}$ radical, a possible mechanism related to the active $\cdot\text{OH}$ radicals in the meso- CuFe_2O_4 system is proposed. Firstly, imidacloprid was adsorbed on the surface of meso- CuFe_2O_4 . Once H_2O_2 was added, $\cdot\text{OH}$ radicals were generated by active sites including Cu(II) and Fe(III) on the catalyst surface. Then the generated $\cdot\text{OH}$ radicals reacted with imidacloprid both adsorbed on the catalyst surface and dissolved in the bulk solution, leading degradation and further mineralization of pollutants. According to Eq. (5), the Fe^{3+} reduction by Cu^+ is thermodynamically favorable, which is benefit for the redox cycles of $\text{Fe}^{2+}/\text{Fe}^{3+}$ and $\text{Cu}^+/\text{Cu}^{2+}$ in meso- CuFe_2O_4 . Especially, the meso- CuFe_2O_4 with unique mesoporous structure possesses high surface area, which is contributing to enhance the number of active sites. Therefore, the synergistic effect of Cu and Fe on the surface of meso- CuFe_2O_4 is more conducive to promote the interfacial electron transfer within meso- CuFe_2O_4 . That is the reason that meso- CuFe_2O_4 presents the best catalytic activity for the degradation of imidacloprid.

The TPR measurements were conducted to investigate the oxidation characteristics of all the catalysts. As shown in Fig. 11, two pronounced reduction peaks were observed at 170–190 and

350–580 °C regions for the meso- CuFe_2O_4 . The reduction peak centered at 180 °C is ascribed to the reduction of CuFe_2O_4 to Cu and Fe_2O_3 , and to the subsequent reduction of Fe_2O_3 to Fe_3O_4 . And the peak located at around 530 °C is responsible to the iron oxides continued to be reduced to metallic Fe via FeO . However, the first reduction peaks for con- CuFe_2O_4 shifted to higher temperature (250 °C). The observation suggested that the ordered mesoporous structure remarkable decrease the reduction temperature of CuFe_2O_4 . In other words, meso- CuFe_2O_4 presents higher oxidation capacity than con- CuFe_2O_4 . While for CoFe_2O_4 system, the main peak presented much higher temperature at 550 °C, revealing that the oxidation capacity of CoFe_2O_4 is lower than CuFe_2O_4 system.

3.3. Degradation intermediates, possible degradation pathway and ecotoxicity

It should be emphasized that imidacloprid was completely degraded in this work. However, the mineralization degree was low, indicating that imidacloprid was transformed into other organic compounds. The degradation intermediates of imidacloprid were identified by GC-MS [52]. Besides the parent imidacloprid, seven intermediates were found (see Fig. 12) [52]. Based on the identified intermediates, possible pathways for the degradation of imidacloprid in the tested systems were proposed as shown in Fig. 12. At the first stage of the reaction, imidacloprid may be attacked by $\cdot\text{OH}$ onto different reactions sites, which yield different intermediates (compounds 1 and 2). On the one hand, 6-chloro nicotinaldehyde (compound 2) was oxidation to 6-chloronicotinic acid (compound 3). On the other hand, 1-(6-chloro-3-pyridinyl) methyl-2-imidazolidinone (compound 1) was further attacked by $\cdot\text{OH}$, which lead to the formation of 6-chloronicotinamide (compound 4) and 1-acetylimidazolidin-2-one (compound 5). At the late stage of the reaction, some short-chain molecular such as carboxylic acids (compound 6) and N,N-dimethyl formamide (compound 7) were formed, suggesting that ring cleavage occurred due to the heterocyclic compound attacked by $\cdot\text{OH}$. Subsequent degradation leading to the short-chain molecules were mineralized to CO_2 , water and other inorganic salts.

There are only less than 1% of pesticides used in agriculture actually reaching the crops. The remaining contaminates the land, the air and particularly the water [53]. In the aquatic environment, imidacloprid is highly toxic on an acute basis to aquatic invertebrates. The goal of this work is to decrease the toxic of imidacloprid using heterogeneous Fenton reaction. The results showed that the intermediates produced during the reaction were similar with TiO_2 photocatalysis or photo-Fenton. According to the literature previously reported [53], the degradation intermediates of imidacloprid are less ecotoxic than the original substrate itself.

3.4. Excellent chemical stability and recyclability of catalysts

The catalyst's stability is an important issue that has to be considered. Therefore, the iron leaching ($C_{\text{Fe}^{3+}}$) in solution was detected during the heterogeneous Fenton oxidation, as exhibited in Fig. 13. The results show that the $C_{\text{Fe}^{3+}}$ of meso- CuFe_2O_4 , meso- CoFe_2O_4 , con- CuFe_2O_4 and con- CoFe_2O_4 range from 0.87 to 1.00 mg L^{-1} , all of them are lower than 2 mg L^{-1} , which is the legal limit imposed by the directives of the European Union. Additionally, these samples possessed much lower leaching degree than nano- Fe_3O_4 (2.3 mg L^{-1}) and the values (9.8 mg L^{-1} for Fe_3O_4 magnetic nanoparticles after 180 min) reported previously [29]. This means the treated contaminants can be directly discharged into the sewage system. From the view of long-term industrial application, spinel based heterogeneous Fenton-like catalysts with such

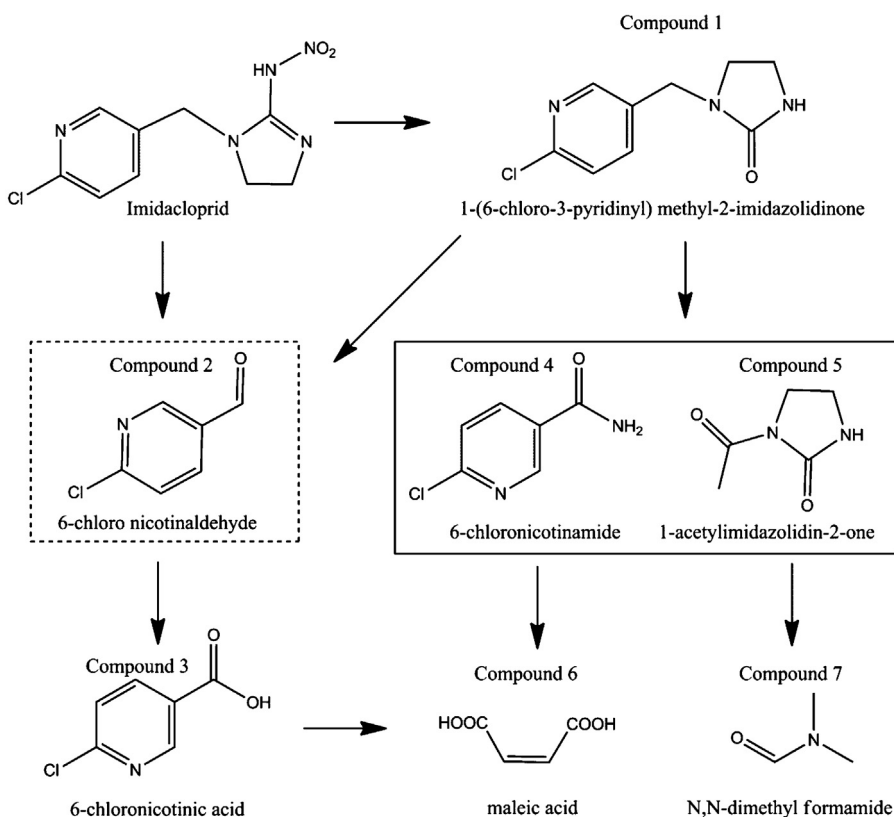


Fig. 12. The proposed degradation pathway for imidacloprid using meso- CuFe_2O_4 as heterogeneous Fenton catalyst.

low iron leaching levels are more cost-effective and practicable in a plant-scale operation.

Undoubtedly, reusability is also an important factor for the application of catalyst in economic perspective. Successive experiments were performed to evaluate the possibility of catalyst reuse. As exhibited in Fig. 14, it is obviously observed that the meso- CuFe_2O_4 remain efficient catalytic activity even after 5 consecutive runs at the same reaction conditions. In addition, the surface morphology of meso- CuFe_2O_4 after reaction, remained the same as fresh sample (examined by SEM, not shown). The obtained results demonstrate that the ordered mesoporous meso- CuFe_2O_4 owns

good stability, which is significant for long-term practical application.

Fig. 15 shows the magnetization curve of the samples investigated by VSM at 300 K. The corresponding magnetic parameters including saturation magnetization (M_s), remnant magnetization (M_r), and coercivity (H_c) of the samples were listed in Table 1. It can be found that the influence of the ordered mesoporous structure on the magnetic properties is very obvious. For instance, the M_r of con- CuFe_2O_4 is 5.792 emu g⁻¹, while the meso- CuFe_2O_4 is only 0.215 emu g⁻¹, suggesting the meso- CuFe_2O_4 is superparamagnetic. The decrease was attributed to the smaller size of meso- CuFe_2O_4 than the con- CuFe_2O_4 , which is consistent with the results of XRD and TEM. The reason is that, if the particle size is smaller than the critical size, the material will show superparamagnetic behavior [54]. The lower H_c values of meso- CuFe_2O_4 suggest

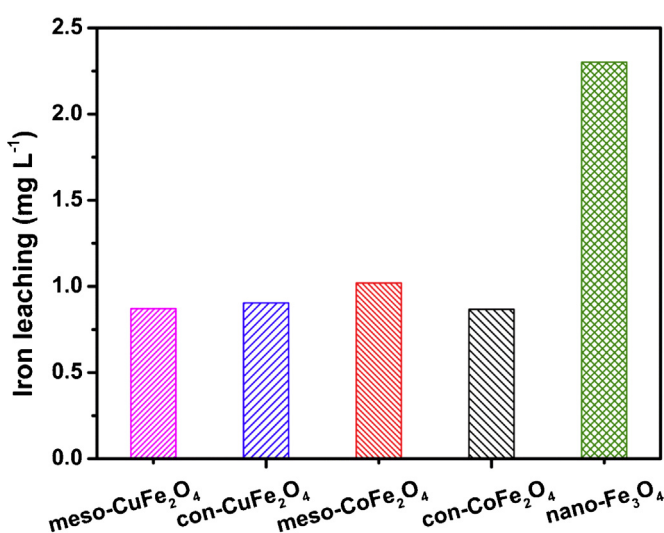


Fig. 13. The concentration of iron leaching in solution during imidacloprid degradation in 5 h, at pH 3.00 with 40 mM H_2O_2 , 0.3 g L⁻¹ catalyst dosage.

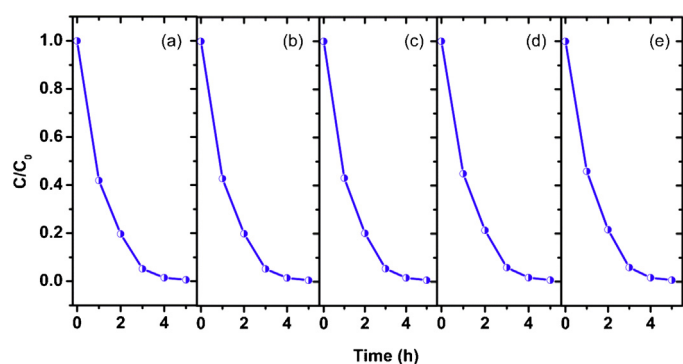


Fig. 14. Degradation of imidacloprid in different batch runs in the H_2O_2 -meso- CuFe_2O_4 system. (a) First use, (b) second use, (c) third use, (d) fourth use, and (e) fifth use (reaction conditions: 10 mg L⁻¹ imidacloprid, 40.0 mM H_2O_2 , 0.3 g L⁻¹ meso- CuFe_2O_4 and pH 3.00).

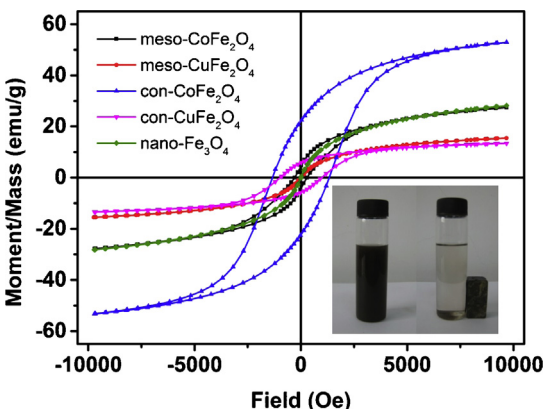


Fig. 15. Hysteresis curves of different catalysts (meso-CuFe₂O₄, meso-CoFe₂O₄, con-CuFe₂O₄, con-CoFe₂O₄ and nano-Fe₃O₄) at room temperature and the photograph of the sample attracted by a magnet (inset).

that they can be separated easily by a magnet. In addition, they can be easily re-dispersed for reuse after separating, because of their low M_r values [30]. These results show that the meso-CuFe₂O₄ and meso-CoFe₂O₄ can be manipulated by an external magnetic field, such as a magnet (Fig. 15, inset), thus providing a potential advantage for the separation, recovery and reuse of catalysts.

4. Conclusions

The ordered mesoporous CuFe₂O₄ was successfully synthesized by using KIT-6 as template through the hard template strategy, and used as heterogeneous Fenton-like catalyst for removing imidacloprid in the presence of H₂O₂. The obtained results show that meso-CuFe₂O₄ possesses highly ordered mesoporous structure, and its surface area and the average pore size are up to 122 m² g⁻¹ and 9.2 nm, respectively. The catalytic activity of heterogeneous catalysts was estimated by the degradation of imidacloprid. The results show that the degradation of imidacloprid follows the pseudo-first order reaction kinetics, and the apparent rate constant of meso-CuFe₂O₄ is 1.0445 h⁻¹, which is 1.5, 2 and 2.5 times than those of con-CuFe₂O₄, meso-CoFe₂O₄ and nano-Fe₃O₄. Three conclusions summarized based on the results of the degradation of imidacloprid and the amount of •OH radicals. Firstly, the catalytic activity of catalysts with ordered mesoporous structure is superior to non-mesoporous structure, suggesting the high efficiency of catalysts is related with their high surface area and large pore size. Secondly, the catalytic activity of CuFe₂O₄ is better than that of CoFe₂O₄. Thirdly, meso-CuFe₂O₄ and meso-CoFe₂O₄ present higher catalytic activity than conventional catalyst such as Fe₃O₄. Moreover, the amount of •OH radicals produced by meso-CuFe₂O₄ is 130 μ mol L⁻¹ in 5 h, and the oxidation states of copper and iron on the surface of meso-CuFe₂O₄ partially change from Cu(II) to Cu(I) and Fe(III) to Fe(II) after the reaction. Based on the above results, a plausible mechanism is proposed. The Fe³⁺ reduction by Cu⁺ is thermodynamically favorable, which is benefit for the redox cycles of Fe²⁺/Fe³⁺ and Cu⁺/Cu²⁺ in meso-CuFe₂O₄. Especially, the meso-CuFe₂O₄ with unique mesoporous structure possesses high surface area, which contributes to enhancing the number of active sites. Therefore, the synergistic effect of Cu and Fe on the surface of meso-CuFe₂O₄ is more conducive to promote the interfacial electron transfer within meso-CuFe₂O₄. In addition, the meso-CuFe₂O₄ presents very low iron leaching, and 5 cyclic tests show that the magnetic catalyst is very stable, recoverable and easy to separate using a magnet. Hence, this magnetic catalyst provides a potential advantage in organic pollutant removal.

Acknowledgements

This work was supported jointly by the National Natural Science Foundation, P.R. China (Project No. 21277099, 21207101), Shanghai Municipal Education Commission and Shanghai Educational Development Foundation (Project No. 2011CG19) and the Program for Young Excellent Talents in Tongji University (Project No. 2010KJ063).

References

- [1] Y.Y. Zhang, J.H. Deng, C. He, S.S. Huang, S.H. Tian, Y. Xiong, Environmental Technology 31 (2010) 145–154.
- [2] L.Xu, J. Wang, Environmental Science and Technology 46 (2012) 10145–10153.
- [3] S. Navalon, A. Dhakshinamoorthy, M. Alvaro, H. Garcia, ChemSusChem 4 (2011) 1712–1730.
- [4] N. Wang, L.H. Zhu, D.L. Wang, M.Q. Wang, Z.F. Lin, H.Q. Tang, Ultrasonics Sonochemistry 17 (2010) 526–533.
- [5] J. Deng, Y. Wen, Q. Wang, Materials Research Bulletin 47 (2012) 3369–3376.
- [6] R.C.C. Costa, M. de Fatima, F. Lelis, L.C.A. Oliveira, J.D. Fabris, J.D. Ardisson, R.R.V.A. Rios, C.N. Silva, R.M. Lago, Catalysis Communications 4 (2003) 525–529.
- [7] R.C.C. Costa, M.F.F. Lelis, L.C.A. Oliveira, J.D. Fabris, J.D. Ardisson, R.R.V.A. Rios, C.N. Silva, R.M. Lago, Journal of Hazardous Materials 129 (2006) 171–178.
- [8] F. Magalhaes, M.C. Pereira, S.E.C. Botrel, J.D. Fabris, W.A. Macedo, R. Mendonca, R.M. Lago, L.C.A. Oliveira, Applied Catalysis A: General 332 (2007) 115–123.
- [9] S.J. Yang, H.P. He, D.Q. Wu, D. Chen, X.L. Liang, Z.H. Qin, M.D. Fan, J.X. Zhu, P. Yuan, Applied Catalysis B: Environmental 89 (2009) 527–535.
- [10] X.L. Liang, Y.H. Zhong, S.Y. Zhu, J.X. Zhu, P. Yuan, H.P. He, J. Zhang, Journal of Hazardous Materials 181 (2010) 112–120.
- [11] X.L. Liang, S.Y. Zhu, Y.H. Zhong, J.X. Zhu, P. Yuan, H.P. He, J. Zhang, Applied Catalysis B: Environmental 97 (2010) 151–159.
- [12] X.L. Liang, Y.H. Zhong, S.Y. Zhu, L.Y. Ma, P. Yuan, J.X. Zhu, H.P. He, Z. Jiang, Journal of Hazardous Materials 199 (2012) 247–254.
- [13] X.L. Liang, Y.H. Zhong, H.P. He, P. Yuan, J.X. Zhu, S.Y. Zhu, Z. Jiang, Chemical Engineering Journal 191 (2012) 177–184.
- [14] H.Y. Niu, D. Zhang, S.X. Zhang, X.L. Zhang, Z.F. Meng, Y.Q. Cai, Journal of Hazardous Materials 190 (2011) 559–565.
- [15] S.T. Xing, Z.C. Zhou, Z.C. Ma, Y.S. Wu, Applied Catalysis B: Environmental 107 (2011) 386–392.
- [16] T. Valdes-Solis, P. Valle-Vigón, S. Alvarez, G. Marban, A.B. Fuertes, Catalysis Communications 8 (2007) 2037–2042.
- [17] D.N. Thi, H.P. Ngoc, H.D. Manh, T.N. Kim, Journal of Hazardous Materials 185 (2011) 653–661.
- [18] S.C. Yang, W.N. Su, S.D. Lin, J. Rick, J.H. Cheng, J.Y. Liu, C.J. Pan, D.G. Liu, J.F. Lee, T.S. Chan, H.S. Sheu, B.J. Hwang, Applied Catalysis B: Environmental 106 (2011) 650–656.
- [19] Y.B. Ding, L.H. Zhu, N. Wang, H.Q. Tang, Applied Catalysis B: Environmental 129 (2013) 153–162.
- [20] T. Zhang, H. Zhu, J.P. Croue, Environmental Science and Technology 47 (2013) 2784–2791.
- [21] Y. Deng, J. Wei, Z. Sun, D. Zhao, Chemical Society Reviews 42 (2013) 4054–4070.
- [22] M.H. Su, C. He, V.K. Sharma, M. Abou Asi, D. Xia, X.Z. Li, H.Q. Deng, Y. Xiong, Journal of Hazardous Materials 211 (2012) 95–103.
- [23] B. Sahoo, S.K. Sahu, S. Nayak, D. Dhara, P. Pramanik, Catalysis Science & Technology 2 (2012) 1367–1374.
- [24] S. Malato, J. Caceres, A. Agüera, M. Mezcuia, D. Hernando, J. Vial, A.R. Fernández-Alba, Environmental Science and Technology 35 (2001) 4359–4366.
- [25] F. Kleitz, S.H. Choi, R. Ryoo, Chemical Communications (2003) 2136–2137.
- [26] H. Yen, Y. Seo, R. Guillet-Nicolas, S. Kaliaguine, F. Kleitz, Chemical Communications 47 (2011) 10473–10475.
- [27] S.X. Zhang, X.L. Zhao, H.Y. Niu, Y.L. Shi, Y.Q. Cai, G.B. Jiang, Journal of Hazardous Materials 167 (2009) 560–566.
- [28] M.E. Lindsey, M.A. Tarr, Chemosphere 41 (2000) 409–417.
- [29] L.J. Xu, J.L. Wang, Applied Catalysis B: Environmental 123 (2012) 117–126.
- [30] T.D. Nguyen, N.H. Phan, M.H. Do, K.T. Ngo, Journal of Hazardous Materials 185 (2011) 653–661.
- [31] J.Y. Feng, X.J. Hu, P.L. Yue, Environmental Science and Technology 38 (2004) 5773–5778.
- [32] Y.Y. Sun, G.B. Ji, M.B. Zheng, X.F. Chang, S.D. Li, Y. Zhang, Journal of Materials Chemistry 20 (2010) 945–952.
- [33] R.K. Selvan, C.O. Augustin, L.J. Berchmans, R. Saraswathi, Materials Research Bulletin 38 (2003) 41–54.
- [34] C. Cannas, A. Ardu, A. Musinu, D. Peddis, G. Piccaluga, Chemistry of Materials 20 (2008) 6364–6371.
- [35] A.L. Andrade, D.M. Souza, M.C. Pereira, J.D. Fabris, R.Z. Domingues, Journal of Nanoscience and Nanotechnology 9 (2009) 3695–3699.
- [36] R. Sathyamoorthy, K. Mageshwari, Physica E: Low-Dimensional Systems & Nanostructures 47 (2013) 157–161.
- [37] T. Valdes-Solis, P. Tartaj, G. Marban, A.B. Fuertes, Nanotechnology 18 (2007) 145603.
- [38] P. Chandramohan, M.P. Srinivasan, S. Velmurugan, S.V. Narasimhan, Journal of Solid State Chemistry 184 (2011) 89–96.

[39] H.C. Choi, Y.M. Jung, S.B. Kim, *Vibrational Spectroscopy* 37 (2005) 33–38.

[40] J.H. Deng, J.Y. Jiang, Y.Y. Zhang, X.P. Lin, C.M. Du, Y. Xiong, *Applied Catalysis B: Environmental* 84 (2008) 468–473.

[41] L.L. Zhang, Y.L. Nie, C. Hu, J.H. Qu, *Applied Catalysis B: Environmental* 125 (2012) 418–424.

[42] S.H. Tian, Y.T. Tu, D.S. Chen, X. Chen, Y. Xiong, *Chemical Engineering Journal* 169 (2011) 31–37.

[43] R.A. Torres, F. Abdelmalek, E. Combet, C. Petrier, C. Pulgarin, *Journal of Hazardous Materials* 146 (2007) 546–551.

[44] R. Zabar, T. Komel, J. Fabjan, M.B. Kralj, P. Trebse, *Chemosphere* 89 (2012) 293–301.

[45] R. Gonzalez-Olmos, M.J. Martin, A. Georgi, F.D. Kopinke, I. Oller, S. Malato, *Applied Catalysis B: Environmental* 125 (2012) 51–58.

[46] S.J. Yang, H.P. He, D.Q. Wu, D. Chen, Y.H. Ma, X.L. Li, J.X. Zhu, P. Yuan, *Industrial & Engineering Chemistry Research* 48 (2009) 9915–9921.

[47] Y.J. Wang, H.Y. Zhao, J.X. Gao, G.H. Zhao, Y.G. Zhang, Y.L. Zhang, *Journal of Physical Chemistry C* 116 (2012) 7457–7463.

[48] C. Reitz, C. Suchomski, J. Haetge, T. Leichtweiss, Z. Jaglicic, I. Djerdj, T. Brezesinski, *Chemical Communications* 48 (2012) 4471–4473.

[49] Z.J. Gu, X. Xiang, G.L. Fan, F. Li, *Journal of Physical Chemistry C* 112 (2008) 18459–18466.

[50] F. Ji, C.L. Li, J.H. Zhang, L. Deng, *Journal of Hazardous Materials* 186 (2011) 1979–1984.

[51] S.S. Lin, M.D. Gurol, *Environmental Science and Technology* 32 (1998) 1417–1423.

[52] Y.J. Wang, H.Y. Zhao, S.N. Chai, Y.B. Wang, G.H. Zhao, D.M. Li, *Chemical Engineering Journal* 223 (2013) 524–535.

[53] V. Kitsiou, N. Filippidis, D. Mantzavinos, I. Pouios, *Applied Catalysis B: Environmental* 86 (2009) 27–35.

[54] X.B. Yan, J.T. Chen, Q.J. Xue, P. Miele, *Microporous and Mesoporous Materials* 135 (2010) 137–142.